Journal of Fluids and Structures (1997) **11,** 247–269

STEADY TWO-DIMENSIONAL TRANSONIC ANALYSIS USING A BOUNDARY INTEGRAL EQUATION METHOD

U. Iemma and L. Morino
Dipartimento di Ingegneria Meccanica e Industriale, University of Rome III Rome, Italy

(Received 3 July 1996)

A boundary integral equation method for the simulation of two-dimensional steady transonic potential flows is presented. The method is based on a conservative differential full-potential formulation. The steady two-dimensional formulation is obtained as the limiting case of the unsteady three-dimensional one, as the iterative method used to obtain steady-state results is a pseudo-time-accurate three-dimensional technique. In the present formulation the full-potential equation appears in the form of a nonlinear wave equation for the velocity potential. All the nonlinear terms, which are expressed in conservative form, are moved to the right-hand side, and treated formally as nonhomogeneous terms. The paper includes a historical review on the development of integral formulations for transonic analysis. Numerical results are obtained for steady two-dimensional transonic flows. Comparisons with existing finite-difference, finite-element, and finite-volume results shows a good agreement. The convergence analysis for an increasing number of grid elements reveals a limit behaviour in good agreement with other numerical methods in both subcritical and supercritical problems. Finally, we present numerical results to demonstrate a remarkable feature of the formulation, that is that the transonic numerical results are quite insensitive to the geometry of the field volume elements; this makes the present formulation particularly appealing for optimal design applications.

1. INTRODUCTION

A boundary integral equation method (BIEM) for the solution of two-dimensional transonic flows is presented. The formulation is based on the work of Iemma (1994) which represents an extension to the conservative full-potential model of the integral formulation of Morino (1974) for potential flows around aircraft having arbitrary shape and motion. Such a formulation has been used for nonlinear TSP (Transonic Small Perturbation) analysis by Tseng & Morino (1982) and Tseng (1983, 1984). Preliminary full-potential results are presented in Morino & Iemma (1993).

In the present work, the emphasis is on the assessment of the method in the two-dimensional analysis, through an investigation of the convergence of the solution of the integral formulation as the mesh size increases, as well as comparisons with numerical results obtained with classical CFD (Computational Fluid Dynamics) methods (i.e., finite-difference, finite-element, and finite-volume). Two different implementations are presented for the numerical evaluation of the nonlinear terms. Both of them are conservative. In a first formulation, the integral term representing the volume nonlinear sources is integrated by parts in order to avoid the evaluation of the divergence of $\nabla\phi$, as in Tseng (1983, 1984) and in Morino & Iemma (1993). In the second one, the volume integral is discretized in its original form. In order to capture shocks, dissipative terms are introduced in the supersonic region of the flow in the

0889–9746/97/030247 + 23 $25.00/fl960076

form of *artificial compressibility,* or linear and nonlinear *artificial viscosity,* or *flux upwinding.* Both formulations are applied here to subcritical and supercritical, steady two-dimensional flows.

A remarkable feature of the method is that, as numerical experiments show, transonic results are quite insensitive to the geometry used for the field volume elements. Specifically, nearly identical results are obtained (for a fixed boundary surface discretization) using a field discretization generated from different boundary geometries. Conversely, one could use the same field discretization for different boundary geometry; this implies that in those applications where repeated calculations are required, the evaluation of the field-to-field coefficients (a very expensive portion of the algorithm) need not be repeated. This property makes the present formulation particularly appealing for optimal design applications.

In Section 2 a historical review on the development of numerical simulation of transonic flows is presented so as to place the present work in the proper context. Section 3 deals with the boundary integral formulation for full-potential unsteady, three-dimensional flows (for the steady, two-dimensional formulation is obtained as the limiting case of the unsteady three-dimensional one, since the iterative method used to obtain steady-state results is a pseudo-time-accurate technique); even if the formulation may be extended to unsteady flows around bodies in arbitrary motion (see Section 2), here we make the assumption that the body moves in uniform translation. The treatment of the nonlinearities is also presented in Section 3. The numerical discretization is briefly outlined in Section 4, whereas, the artificial dissipation schemes are discussed in Section 5. The numerical results for two-dimensional steady-state flows are presented in Section 6, and compared with finite-element, finite-difference, and finite-volume solutions of both the full-potential and (when applicable) Euler equations. The results of the convergence analysis as well as the field grid insensitivity are included in Section 6. The theoretical aspects of the present work have been developed jointly by the two authors; the numerical results have been obtained by the first author.

2. RELATIONSHIP WITH EXISTING WORK

In the last 20 years, the numerical simulation of transonic flows has been one of the most active fields of research in Computational Fluid Dynamics (CFD). Thus, an exhaustive review of the work performed is beyond the scope of the present paper. On the other hand, the contribution of the present work is better understood within the more general framework of CFD. In this section we present a brief historical review of the development of numerical methods for transonic potential flows, with emphasis on boundary integral formulation considered here. For completeness, we first recall some milestones in the development of CFD methods for transonic flows [for reviews in the field see Hirsh (1990)].

A finite-difference solution of the nonlinear equation for the potential in the transonic range was first obtained in Murman & Cole (1971), which is to be considered a milestone in the development of numerical techniques for the solution of transonic flows. The basic idea of this work is the introduction of a *type-dependent* differencing scheme, which ensures that the domain of dependence of the finite-difference equations is closely related to that of the original differential equation. In order to achieve this, the derivative of the potential in the flow direction is approximated by upwind differences within the supersonic region of the field, whereas central differences are used for the subsonic points. This original idea has been extended by Murman (1974)

to conservative TSP, and to the full-potential equation by Jameson (1974, 1975), for both the nonconservative and the conservative forms of the equation. A different interpretation of the artificial dissipation terms results if one includes the dissipative effects only in the evaluation of the density; this point of view, first proposed by Eberle (1977) and generalized by Hafez *et al.* (1978) and Holst & Ballhaus (1979), is known as *artificial compressibility,* and has been successfully applied in the past to the finite-element solution of the full-potential equation. Another approach to the treatment of the hyperbolic region of the domain is based on the modification of the mass flux in the field by means of an upwind biasing evaluation. This class of dissipation schemes derives from an accurate reformulation of the artificial-dissipation concepts for developing monotone converging schemes for the numerical solution of the Euler equation. The first applications of this technique are due to Engquist & Osher (1980) for the small-disturbance equation, and to Osher (1982) for the full-potential equation.

Next, we turn our attention on the transonic-flow analysis based on boundary integral methods. Boundary integral equations were used for the analysis of transonic aerodynamics in the pioneering work of Oswatitsch (1950) [which precedes by over 20 years the finite-difference work of Murman & Cole (1971)] and Spreiter & Alskne (1954), for steady, two-dimensional, transonic flows. Nixon (1974, 1978) presents a perturbation scheme for the solution of unsteady two-dimensional and steady three-dimensional flows, respectively. In Piers & Sloof (1979) a shock capturing integral formulation is applied to the TSP model.

Next, consider the formulation used here. This is based on that proposed by Morino (1974) and implemented by Tseng & Morino (1982) for the TSP case. This formulation was applied by Tseng (1983, 1984) to steady two- and three-dimensional flows. Applications closely related to the approach of Tseng & Morino (1982), have been presented by Iemma *et al.* (1991) who present a validation for three-dimensional unsteady flows. In the above papers, a simple upwind-difference scheme is used for the evaluation of $\partial\phi/\partial x$ in the field sources for the supersonic points of the flow field [akin to the type-dependent scheme of Murman & Cole (1971)]. Conservative artificial dissipation schemes are introduced in Morino & Iemma (1993) and further developed in Iemma (1994) and in Iemma & Morino (1994). These papers introduce the dissipative effects in the full-potential equation in the form of linear and nonlinear *artificial viscosity,* as well as *artificial compressibility* or *flux-upwinding.* The numerical results are in good agreement with other CFD methods (finite differences, finite volumes, and finite elements). Preliminary results obtained in aeroelastic applications using the full-potential integral formulation are included in Morino *et al.* (1994) whereas applications to the aerodynamic and aeroacoustic analysis of helicopter rotors in hover are presented in Morino *et al.* (1992), Iemma *et al.* (1993) and Gennaretti *et al.* (1995a,b).

The above formulations are oriented towards engineering applications. Here, we examine in-depth some properties of the methodology. Specifically, we present a systematic analysis of the convergence as the number of elements increase (with converged solution properties obtained by extrapolation), thereby obtaining a meaningful comparison with existing results. Also, the convergence of the iterative scheme is addressed carefully. Finally, we present novel results regarding the issue of field-grid independence (which makes the methodology particularly attractive for design applications, as explained above).

Finally, for completeness, consider some related and independently developed BEM formulations. As mentioned above, a steady full-potential formulation has been

proposed by Sinclair (1986, 1988) and applied to two-dimensional and three-dimensional configurations, respectively. In contrast to Tseng & Morino (1982) (and all the subsequent papers cited above) where the field sources include exclusively nonlinear terms, in Sinclair (1986, 1988) the field sources include all the compressibility terms (linear and nonlinear); this implies that the differential operator for the boundary integral formulation of Tseng & Morino (1982) is that of the wave equation, whereas for Sinclair (1986, 1988) it is the Laplacian and, as a consequence, field integrals are required even for the linear case (subsonic flows). A shock-capturing shock-fitting (SCSF) scheme has been introduced by Kandil & Hu (1988), who use an integral formulation similar to that of Sinclair (1986, 1988) for the shock capturing part of the algorithm, whereas a shock fitting procedure is introduced by evaluating the shock strength and orientation using the Rankine–Hugoniot relations; the integral equation is modified by introducing a source distribution on the shock surface, with intensity proportional to the local shock strength. The work of Kandil & Hu (1988) also includes the solution of the Euler equations by coupling the integral formulation with a finite difference solution of the Euler equation within a domain surrounding the shock. A formulation closely related to that of Sinclair (1988) [i.e., including all the compressibility effects as a sources distribution in the floe field] is presented by Röttgermann & Wagner (1995a, b), and Zhang *et al.* (1995) who extend this type of approach to the analysis of helicopter rotors in the transonic regime, including the effects of the rolled-up wake geometry. They use a full-potential equation written in nonconservative form; this is not to be considered a strong limitation, since, in helicopter applications, shock waves are typically weak. Indeed, their work represents probably the most advanced application of those integral formulations that are based on the Laplacian.

3. FULL POTENTIAL INTEGRAL FORMULATION

Consider first the differential formulation of the problem [for details see Morino & Iemma (1993), or Morino (1993)]. The equation governing the motion of an isentropic irrotational flow is the full-potential equation, which is obtained by combining the conservative form of the continuity equation with Bernoulli's theorem for isentropic potential compressible flow, and taking into account the isentropic density–enthalpy relation. In a frame of reference rigidly connected with the body (BFR) this is given by

$$\nabla^2\phi - \frac{1}{a_\infty^2}\frac{d_B^2\phi}{dt^2} = \sigma, \tag{1}$$

where σ represents all the nonlinear terms, whereas $d_B/dt := \partial/\partial t - \mathbf{v}_B \cdot \nabla$ is the time derivative written in the BFR (where $\mathbf{v}_B$ is the velocity of the point of the BFR), i.e., following a point fixed in the air frame of reference. The expression for σ is

$$\sigma = \nabla \cdot \mathbf{b} + \frac{\partial \hat{b}}{\partial t}, \tag{2}$$

where

$$\mathbf{b} = \left(1 - \frac{\rho}{\rho_\infty}\right)\nabla\phi - \mathbf{v}_B\hat{b} \quad \text{and} \quad \hat{b} = \frac{\rho}{\rho_\infty} + \frac{1}{a_\infty^2}\frac{d_B\phi}{dt}, \tag{3}$$

with ρ/ρ_∞ obtained from the Bernoulli theorem as $\rho/\rho_\infty = [1 - 1/h_\infty(d_B\phi/dt + v^2/2)]^{1/\gamma-1}$. Different expressions (small-disturbance; nonconservative) for the nonlinear terms σ are discussed in Morino & Iemma (1993).

The boundary conditions complete the differential problem. These are (Morino & Iemma 1993; Morino 1993) the impermeability of the body surface $\mathscr{S}_B$, or

$$\frac{\partial \phi}{\partial n} = \mathbf{v}_B \cdot \mathbf{n}, \qquad \text{for } \mathbf{x} \text{ on } \mathscr{S}_B, \tag{4}$$

and $\phi = 0$ at infinity. In addition, we have the conditions of impermeability and of pressure continuity across the wake surface, $\mathscr{S}_W$. These yield, for $\mathbf{x}$ on $\mathscr{S}_W$,

$$\Delta\left(\frac{\partial \phi}{\partial n}\right) = 0, \tag{5}$$

$$\frac{D_W}{Dt}(\Delta\phi) = 0, \tag{6}$$

with $D_W/Dt := \partial/\partial t + \mathbf{v}_W \cdot \boldsymbol{\nabla}$, where $\mathbf{v}_W$ is the velocity of a point of the wake. Equation (6) states that $\Delta\phi$ is constant in time following a wake point $\mathbf{x}_W$ and equal to the value it had when $\mathbf{x}_W$ left the trailing edge. This is obtained from the condition that $\Delta\phi_W = \Delta\phi_B$ at the trailing edge. In addition, we assume homogeneous initial conditions.

The integral formulation for the above differential problem is outlined in the following. In the present paper we deal with applications to fixed-wing analysis; thus, the integral equation presented is limited to bodies in uniform translation. In this case $\mathbf{v}_B = \{-U_\infty, 0, 0\}$ and $d_b/dt = \partial/\partial t + U_\infty \partial/\partial x$.

The fundamental solution G for equation (1) is the solution of the problem

$$\nabla^2 G - \frac{1}{a_\infty^2}\frac{d_B^2 \phi}{dt^2} G = \delta(\mathbf{x} - \mathbf{x}_*)\delta(t - t_*), \tag{7}$$

where δ denotes the Dirac delta function. The "initial" conditions and the boundary condition at infinity associated with the above problem are, respectively, $G(\mathbf{x}, \infty) = \dot{G}(\mathbf{x}, \infty) = 0$, and $G(\infty, t) = 0$. The expression of G for $M_\infty = U_\infty/a_\infty < 1$ (subsonic undisturbed flow) flows is (Morino 1974)

$$G(\mathbf{x}, \mathbf{x}_*, t, t_*) = \frac{-1}{4\pi r_\beta}\,\delta(t - t_* + \theta), \tag{8}$$

where $r_\beta(\mathbf{x}, \mathbf{x}_*) = \sqrt{M_\infty^2(x - x_*)^2 + \beta^2 r^2}$ and $\theta(\mathbf{x}, \mathbf{x}_*) = [r_\beta + M_\infty(x - x_*)]/a_\infty\beta^2$ with $\beta = \sqrt{1 - M_\infty^2}$ and $r = \|\mathbf{r}\| = \|\mathbf{x} - \mathbf{x}_*\|$.

The integral formulation of the problem is obtained by multiplying equation (1) by G and equation (7) by ϕ, subtracting, and integrating in time and over the entire domain $\mathscr{V}$. Applying the Gauss theorem, using the boundary condition at infinity for G and ϕ, integrating with respect to time (taking into account the initial conditions on ϕ and G), and introducing the Prandtl-Glauert variables, $x_0 = x/\beta$, $y_0 = y$, $z_0 = z$, yields

$$\begin{aligned}\phi(\mathbf{x}_{0_*}, t_*) = &\oiint_{\mathscr{S}_{B_0}} \left[G_0 \frac{\partial \phi}{\partial n_0} - \phi \frac{\partial G_0}{\partial n_0} + \frac{\partial \phi}{\partial t} G_0 \frac{\partial \hat{\theta}_0}{\partial n_0}\right]^{\theta_0} \mathrm{d}\mathscr{S}_0 \\ &- \iint_{\mathscr{S}_{W_0}} \left[\Delta\phi \frac{\partial G_0}{\partial n_0} - \Delta\dot{\phi} G_0 \frac{\partial \hat{\theta}_0}{\partial n_0}\right]^{\theta_0} \mathrm{d}\mathscr{S}_0 + \iiint_{\mathscr{V}_0} G_0[\sigma]^{\theta_0}\,\mathrm{d}\mathscr{V}_0,\end{aligned} \tag{9}$$

where $G_0 = -1/4\pi r_0$, with $r_0 = \|\mathbf{x}_0 - \mathbf{x}_{0_*}\|$, whereas $[\ldots]^{\theta_0}$ denotes evaluation at the

retarded time $t = t_* - \theta_0$, with $\theta_0 = [r_0 + M_\infty(x_0 - x_{0_*})]/a_\infty\beta$. Moreover, $\mathscr{S}_{B_0}$ and $\mathscr{S}_{W_0}$ are images of the surfaces of the body and of the wake in the Prandtl-Glauert space, whereas $\partial/\partial n_0$ denotes the corresponding normal derivative, and $\hat{\theta}_0 = [r_0 - M_\infty(x_0 - x_{0_*})]/a_\infty\beta$. Also, $\sigma = \nabla_0 \cdot \mathbf{b}_0 + \partial\hat{b}/\partial t$ with $\mathbf{b}_0 = (b_x/\beta)\mathbf{i} + b_y\mathbf{j} + b_z\mathbf{k}$.

If $\sigma = 0$ (i.e., in the linear subsonic case) and $\mathbf{x}_{0^*} \in \mathscr{V}$, equation (9) is an integral representation for $\phi(\mathbf{x}_{0_*}, t_*)$ as a function of ϕ, $\partial\phi/\partial n_0$ on $\mathscr{S}_{B_0}$ and of $\Delta\phi$ on $\mathscr{S}_{W_0}$. On the other hand, if $\mathbf{x}_{0_*}$ is on $\mathscr{S}_B$, equation (9) represents a compatibility condition between ϕ and $\partial\phi/\partial n_0$ on $\mathscr{S}_{B_0}$ and $\Delta\phi$ on $\mathscr{S}_{W_0}$ for any function ϕ satisfying equation (1). Since $\partial\phi/\partial n$ is known from the boundary conditions, and $\Delta\phi$ from the preceding time history, equation (9) corresponds to a boundary integral equation for ϕ.

In the nonlinear case ($\sigma \neq 0$), the method of solution is similar. Indeed, we take advantage of the evolution of nonlinear terms at retarded times and hence only the current value of σ needs to be evaluated (by numerical differentiation) from ϕ in the field.

Two different approaches are introduced for the numerical evaluation of the volume integral of equation (9). In the first one [following Tseng (1983)] an integration by parts of the nonlinear terms integral is introduced, so as to avoid the evaluation of the divergence operator. Specifically, considering that $[\nabla_0 \cdot \mathbf{b}_0]^{\theta_0} = \nabla_0 \cdot [\mathbf{b}_0]^{\theta_0} + [\partial\mathbf{b}_0/\partial t]^{\theta_0} \cdot \nabla\theta_0$ and applying the divergence theorem, we obtain

$$\iiint_{\mathscr{V}_0} G_0[\sigma]^{\theta_0}\,\mathrm{d}\mathscr{V}_0 = -\oiint_{\mathscr{S}_B} [\mathbf{n}_0 \cdot \mathbf{b}_0]^{\theta_0} G_0\,\mathrm{d}\mathscr{S}_0 - \iiint_{\mathscr{V}_0} [\mathbf{b}_0]^{\theta_0} \cdot \nabla_0 G_0\,\mathrm{d}\mathscr{V}_0 + \iiint_{\mathscr{V}_0} \left[\frac{\partial\hat{b}}{\partial t} + \frac{\partial\mathbf{b}_0}{\partial t} \cdot \nabla_0\theta_0\right]^{\theta_0} G_0\,\mathrm{d}\mathscr{V}_0 \tag{10}$$

This approach, under the assumption of small perturbation, has been applied in the past to the analysis of two- and three-dimensional unsteady transonic flows around fixed and rotary wings (Iemma *et al.* 1991; Morino *et al.* 1992). Here, the same approach is applied to the solution of the full-potential equation for two-dimensional steady problems, because, as mentioned above, the steady two-dimensional formulation is obtained as the limiting case of the unsteady three-dimensional one, since the iterative method used to obtain steady-state results is a pseudo-time-accurate technique.

In the second approach [more recent, introduced by Iemma (1994)] the volume integral is discretized in its original form. This second approach appears to be computationally more convenient than the first one, for reasons indicated in the next section.

4. NUMERICAL DISCRETIZATION

In order to solve the problem numerically, the above integral equation is discretized using a zeroth-order boundary-element formulation. The surface of the body is divided into M elements, $\mathscr{S}_m$, that of the wake into N elements, $\mathscr{S}_n$ and the fluid volume into Q volume elements, $\mathscr{V}_q$. Using the collocation method, and setting the collocation points at the centers of elements, we obtain the discretized version of equation (9), the form

of which depends on the formulation adopted for the field integral. Specifically, combining equations (10) and (9) and discretizing yields

$$\phi_k(t) = \sum_{m=1}^{M} B_{km}[\check{\chi}_m]^{\theta_{0_{km}}} + \sum_{m=1}^{M} C_{km}[\phi_m]^{\theta_{0_{km}}} + \sum_{m=1}^{M} D_{km}[\dot{\phi}_m]^{\theta_{0_{km}}} + \sum_{n=0}^{N} F_{kn}[\Delta\phi_n]^{\theta_{0_{kn}}} + \sum_{n=1}^{N} G_{kn}[\Delta\dot{\phi}_n]^{\theta_{0_{kn}}} + \sum_{q=1}^{Q} \mathbf{H}_{kq} \cdot [\mathbf{b}_{0_q}]^{\theta_{0_{kq}}} + \sum_{q=1}^{Q} \bar{\mathbf{H}}_{kq} \cdot [\dot{\mathbf{b}}_{0_q}]^{\theta_{0_{kq}}} + \sum_{q=1}^{Q} H_{kq}[\dot{\hat{b}}_q]^{\theta_{0_{kq}}}, \tag{11}$$

where $\check{\chi}_m = \partial\phi/\partial n_0 - \mathbf{n}_0(\mathbf{x}_m) \cdot \check{\mathbf{b}}_0(\mathbf{x}_m)$, and $[\ldots]_{\theta_{0_{km}}}$ denotes evaluation at the retarded time $t - \theta_{0_{km}}$; whereas discretizing equation (9) in its original form yields

$$\phi_k(t) = \sum_{m=1}^{M} B_{km}[\chi_m]^{\theta_{0_{km}}} + \sum_{m=1}^{N} C_{km}[\phi_m]^{\theta_{0_{km}}} + \sum_{m=1}^{M} D_{km}[\dot{\phi}_m]^{\theta_{0_{km}}} + \sum_{n=1}^{N} F_m[\Delta\phi_n]^{\theta_{0_{kn}}} + \sum_{n=1}^{N} G_{km}[\Delta\dot{\phi}_n]^{\theta_{0_{km}}} + \sum_{q=1}^{Q} H_{kq}[\sigma_{0_1}]^{\theta_{0_{kq}}}, \tag{12}$$

with $[\sigma_0]^{\theta_0} \approx \overline{\nabla \cdot [\mathbf{b}_0]^{\theta_0}} + [\partial\hat{b}_0/\partial t + \nabla\theta_0 \cdot \partial\mathbf{b}_0/\partial t]^{\theta_0}$, where $\overline{\nabla \cdot [\mathbf{b}_0]^{\theta_0}}$, the mean value of $\nabla \cdot \mathbf{b}_0$ on each element, is calculated as the flux of $\mathbf{b}_0$ through the boundary $\partial\mathscr{V}_q$

$$\overline{\nabla \cdot [\mathbf{b}_0]^{\theta_0}}|_q = \frac{1}{\mathscr{V}_q} \iiint_{\mathscr{V}_q} \nabla \cdot [\mathbf{b}_0]^{\theta_0} \, \mathrm{d}\mathscr{V} = \frac{1}{\mathscr{V}_q} \oiint_{\partial\mathscr{V}_q} \cdot [\mathbf{b}_0]^{\theta_0} \cdot \mathbf{n} \, \mathrm{d}\mathscr{S}, \tag{13}$$

$\mathbf{n}$ being the unit normal to the surface $\partial\mathscr{V}_q$. Note that equation (11) requires the evaluation of seven coefficients for each pair kq (two vector quantities plus a scalar one), whereas only one single scalar is needed in equation (12). Considering that the number of nonlinear coefficients is proportional to the square of the number of elements in the field, we see that equation (12) is more convenient from a numerical point of view, in terms of both computer time and storage space.

5. ARTIFICIAL DISSIPATION

In order to capture shocks, the present formulation utilizes the addition of dissipative effects in the supersonic region of the flows. The conservative artificial dissipation schemes presented here are extensions of the approach in Morino & Iemma (1993) for different forms of the dissipative terms. Four different schemes are considered and applied to the boundary integral equation presented above. When the nonlinear field integral is integrated by parts, the artificial dissipation is included in the form of linear and nonlinear *artificial viscosity,* as well as *artificial compressibility,* whereas a *flux upwinding* technique is applied in the evaluation of $\mathbf{b}_0 \cdot \mathbf{n}$ on $\partial\mathscr{V}_q$, when the field sources are discretized in their original form. All these concepts are adaptations to the boundary integral equation method of existing CFD techniques.

5.1. Artificial Viscosity

A technique for including dissipative effects in the full-potential equation deals with the addition of artificial viscous terms within the supersonic region of flow. These terms should be proportional to upwind derivatives of the velocity in the local direction of the flow. This technique could be considered as a direct evolution of the original *type-dependent differencing,* introduced by Murman & Cole (1971) for the non-conservative TSP equation, extended to conservative TSP by Murman (1974), and to the full-potential equation by Jameson (1974, 1975) for both the nonconservative and the conservative forms of the equation. The adaptation to the present boundary integral equation formulation is considered in two different ways. In the first one, the viscous correction is introduced at the level of the evaluation of the x-component of the velocity. The modified quantity has the form

$$\tilde{u} = \phi_x^c - \Delta s \frac{\partial}{\partial s}\left(\mu \frac{\partial \phi}{\partial x}\right), \tag{14}$$

where ϕ_x^c indicates the centered finite difference approximation for the x-derivative of the potential, and $\mu(M)$ represents the switching function that activates the dissipation terms where $M > 1$. The typical expression suggested in the literature for μ is $\mu(M) = C \max[0, 1 - M_c^2/M^2]$, where M_c is a *cut-off* Mach number, and C is a constant (the use of M_c prevents instabilities at the sonic line due to the discontinuity of the slope of the function $\mu(M) \in \mathscr{C}^0$, by moving the commutation slightly below the sonic point). A new expression for the switching function was introduced by Iemma (1994) in order to achieve the same stability with $M_c = 1$. The function $\mu(M) \in \mathscr{C}^\infty$ is

$$\mu(M) = \frac{C}{1 + \mathrm{e}^{-\lambda(M - M_0)}}, \tag{15}$$

where λ controls the slope of the function at $M = M_0$. The expression of $\tilde{u}$ in equation (14) is introduced in the Bernoulli theorem (to evaluate ρ/ρ_∞), as well as in equation (2). Thus, the dissipative term added to the inviscid nonlinear term is nonlinear.

5.2. Artificial Compressibility

Including the dissipative effects in the calculation of the density, results in a different interpretation of the artificial dissipation terms. This point of view, first proposed by Eberle (1977), generalized by Hafez *et al.* (1978) and Holst & Ballhaus (1979), and known as *artificial compressibility,* has been successfully applied in the past to the finite element solution of the full-potential equation. In adapting this approach to the boundary integral formulation, we consider the modified density

$$\tilde{\rho} = \rho - \mu(M) \Delta s \frac{\partial \rho}{\partial s}, \tag{16}$$

where s is the arc-length in the streamwise direction. The dissipative effects are introduced by substituting ρ with $\tilde{\rho}$ in equation (3).

5.3. Artificial Mass Generation

In the third approach, the artificial viscosity term is introduced as an artificial mass-flux in the evaluation of the nonlinear source terms

$$\tilde{\sigma} = \sigma + \Delta s \frac{\partial}{\partial x}\left[\mu \frac{\partial}{\partial s}\left(\frac{\partial \phi}{\partial x}\right)\right]. \tag{17}$$

After integration by parts, the above expression assumes the form $\tilde{\mathbf{b}}_k = \mathbf{b}_k - \Delta s \mu_k \, \partial u / \partial s|_k \, \mathbf{i}$, where $\mathbf{i}$ represents the unit vector of the x direction. The latter approach yields a linear artificial viscous term. This peculiarity seems to have a favorable influence on the stability of the iteration process.

5.4. Flux Upwinding

If the nonlinear terms are not integrated by parts, the evaluation of $\nabla \cdot \mathbf{b}$ is reduced to the evaluation of the flux of $\mathbf{b}$ through the boundary of each element $\mathscr{V}_q$. The introduction of dissipative terms in such a formulation is accomplished by using a so-called *flux-upwinding* scheme. This class of dissipation schemes, derived from an accurate reformulation of the artificial dissipation concepts, yields monotone converging schemes for the numerical solution of the Euler equation. Early applications of this technique are due to Engquist & Osher (1980) for the small-disturbance equation, and to Osher (1982) for the full-potential equation. A very general form for these schemes can be presented (for two-dimensional flows) by denoting with $f_{i-1/2,j}$, $f_{i+1/2,j}$, $f_{i,j+1/2}$, $f_{i,j-1/2}$ the mass flux flowing through the four faces of the two-dimensional element surrounding the control point $\mathbf{x}_{ij}$, and by identifying i as the index following the local stream direction. Dissipative effects are introduced at supersonic points by means of the modified flux $f^d_{i\pm1/2,j}$:

$$f^d_{i\pm1/2,j} = f_{i\pm1/2,j} - D_{i\pm1/2,j}, \tag{18}$$

where D represents a general form of dissipation. In the present formulation we have $f_{i\pm1/2,j} = \mathbf{b} \cdot \mathbf{n}|_{i\pm1/2,j}$, and for the additive term D a first-order expression is used. We obtain

$$f^d_{i\pm1/2,j} = f_{i\pm1/2,j} - \mu_{i\pm1/2,j} \left. \frac{\partial f}{\partial s} \right|_{i\pm1/2,j} \Delta s \tag{19}$$

6. NUMERICAL RESULTS

The formulation presented above is applied to the analysis of steady two-dimensional transonic flows. Particular emphasis is given to the validation of the algorithm in subcritical and supercritical regimes, through comparisons with existing numerical solutions of the full-potential and Euler equations. Indeed, for subcritical flows the full-potential model is exactly equivalent to the complete Euler model, since no entropy or vorticity sources (such as strong shock waves) are present in the field. Moreover, if only weak shock waves occur, comparisons between the two formulations are still meaningful, since the entropy jump and vorticity introduced by the shock remain negligible.

The applications presented in the following deal with the two approaches presented for the treatment of the nonlinear terms (with and without the integration by parts of the field-source term). Note that the steady solution is obtained by marching in time, and that a two-dimensional problem is approximated by a three-dimensional one with a very high aspect ratio. The results may be divided into five groups. Two-dimensional, steady, subcritical (no shock waves) problems are presented first, and compared to numerical solutions of the Euler equation, in order to assess the algorithm in the absence of dissipation schemes. Two-dimensional steady supercritical problems are then analysed; comparisons with existing numerical solutions of the full potential and Euler equation are presented, including the validation of the dissipation schemes described

above. Then, the effects of the dissipation schemes and of the grid type are considered. Finally, some results demonstrating the independence of the solution from the field grid geometry are presented (as mentioned above, this feature is highly desirable in those applications where repeated calculations are required, such as optimal design of airfoil shapes).

6.1. Subcritical Flows

In order to validate the nonlinear potential model, the present method has been applied to two-dimensional subcritical cases, and compared to numerical solutions of the Euler equation obtained by Lerat & Sides (1986) and Dadone (1986). Two different tests are considered: the flow around a circular cylinder at $M_\infty = 0{\cdot}38$, and a NACA 0012 airfoil at $M_\infty = 0{\cdot}63$ with angle of attack $\alpha = 2°$. These test cases are chosen just below the critical (i.e., sonic) conditions, in order to ensure a strong influence of the nonlinear terms, and, at the same time, to ensure the isentropicity of the flow. The comparison of the pressure distributions obtained for the two test cases confirms the accuracy of the prediction of the present method.

Figure 1 depicts the pressure coefficient distribution on the surface of the cylinder at $M_\infty = 0{\cdot}38$. The solution of the present method is obtained using an O-type grid for the evaluation of the nonlinear field sources, with 60×15 volume elements. The solution for the nonlinear potential problem is compared to that for a linear potential one and to both Euler solutions. The prediction of the nonlinear boundary integral formulation shows quite a good agreement with both Euler solutions. The comparison with the linear potential solution confirms the strong influence of the nonlinear terms. The convergence of the iteration scheme appears to be very fast, as shown in Figure 2. The time history of the quantity $|\sigma_{n+1} - \sigma_n|/|\sigma_1|$ is presented, where n denotes the iteration index. As we will see, the convergence rate appears to depend upon the regularity of the computational mesh. Nonuniform meshes require a higher number of iterations to reach convergence. Indeed, a nonuniform C-type grid is used for the test case of

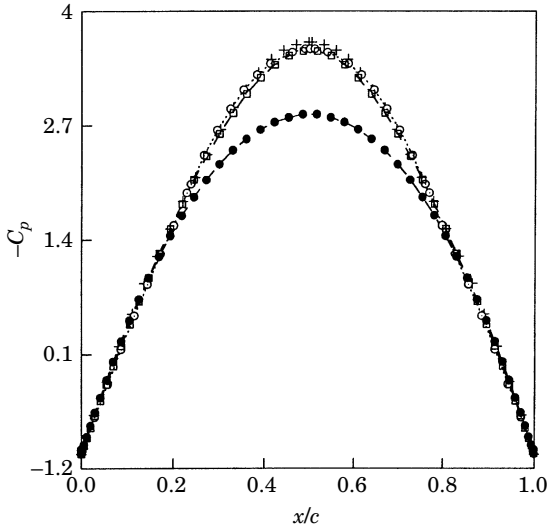

Figure 1. Pressure coefficient distribution on the surface of a unit circle at $M_\infty = 0{\cdot}38$: —●—, BEM linear potential; —□—, BEM non-linear potential; —○—, Euler solution (Lerat & Sides 1986); — + —, Euler solution. (Dadone 1986).

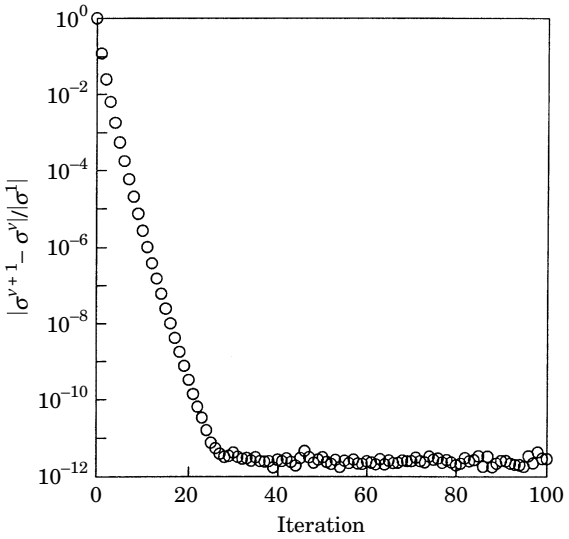

Figure 2. Time history of the iterative procedure. Test case of Figure 1.

Figures 4 and 5 (NACA 0012 airfoil at $M_\infty = 0{\cdot}63$ and angle of attack $\alpha = 2°$), with 40×15 field elements. The solution is still very accurate in terms of pressure distribution when compared to the Euler solutions, but the steady state is reached after a higher number of steps with respect to the uniform grid solution. Nevertheless, this number remains considerably lower than that required by other CFD methods.

In order to evaluate the rate of convergence of the numerical solution as the number of elements increases, the results obtained with different mesh sizes have been compared to the reference numerical solutions of the Euler equations. Results obtained with the convergence analysis are presented in Figures 3 and 6.

The parameter used for the non-lifting flow around the cylinder is the local value of

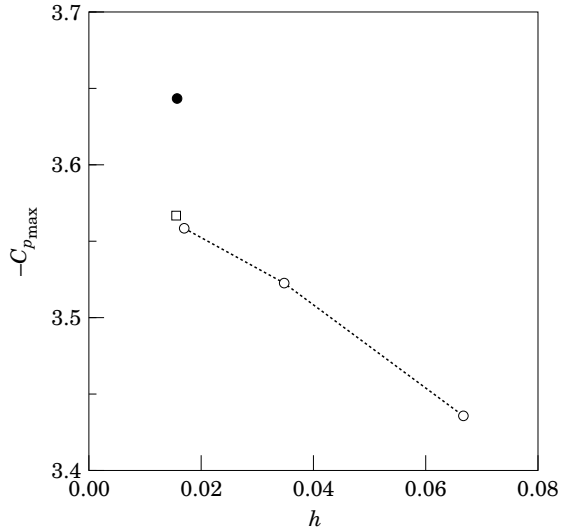

Figure 3. Convergence of the maximum value of the C_p for the case of Figure 1, for increasing number of grid elements, $N(h = 1/N)$: —○—, BEM nonlinear potential; □, Euler solution (Lerat & Sides 1986); ●, Euler solution (Dadone 1986).

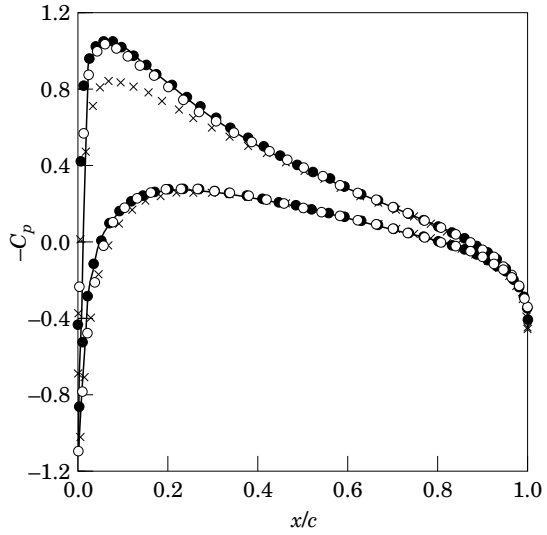

Figure 4. Pressure coefficient distribution on a NACA 0012 airfoil at $M_\infty = 0{\cdot}63$, and angle of attack $\alpha = 2°$: ×, BEM linear potential; ——, Euler solution (Lerat & Sides 1986); —○, BEM nonlinear, equation (10); —●—, BEM nonlinear, equation (13).

pressure coefficients on the body at $\theta = \pi/2$. The boundary integral solution converges to a value close to that predicted by Lerat & Sides (1986). The slight difference with respect to Dadone (1986) (limited within the 3% of the local value of the pressure coefficient, Figure 1) may be due to the fact that such a solution is affected, as stated by that author, by a numerical production of vorticity, even when the flow is potential.

The same analysis has been performed for a lifting flow around a NACA 0012 airfoil. In this case, the parameter used to analyse the convergence of the integral solution is the lift coefficient. When we focus our attention to an integral quantity, such as the lift coefficient, the local small differences between the two reference Euler solutions totally disappear, Figure 6 (the production of spurious vorticity in the reference solution is

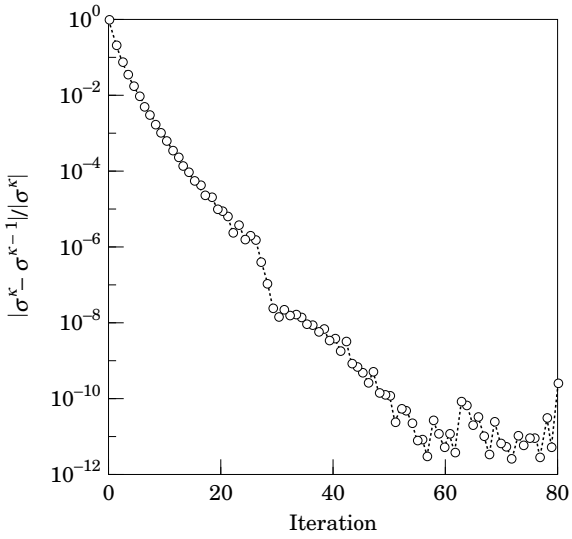

Figure 5. Time history of the iterative procedure. Test case of Figure 4.

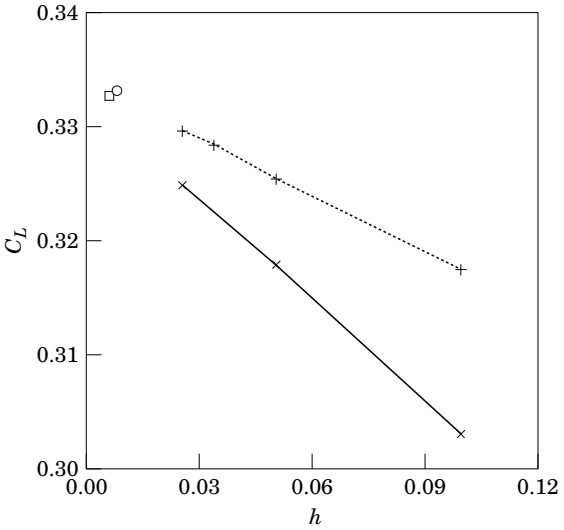

Figure 6. Convergence of the value of the lift coefficient the C_L for the case of Figure 4, for increasing number of grid elements, $N(h = 1/N)$: —+—, BEM nonlinear potential, equation (10); —×—, BEM nonlinear potential, equation (13); —□—, Euler solution (Lerat & Sides 1986); —□—, Euler solution (Dadone 1986).

limited to the region where the local Mach number approaches unity). In the lifting case, presented in Figure 2, the boundary integral solution converges to a value in excellent agremeent with both Euler solutions, and this is true for both numerical treatments of the nonlinear-term integral.

6.2. Supercritical Flows

The present boundary integral method is capable of capturing sharp shocks, when they occur. Figure 7 depicts the pressure distribution on the surface of a cylinder at

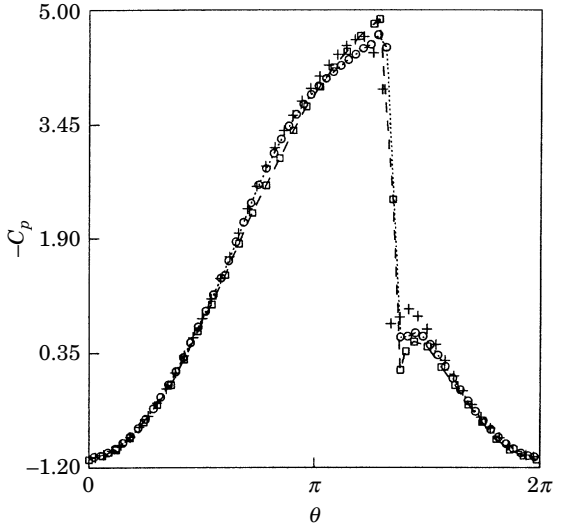

Figure 7. Pressure coefficient distribution on the surface of a unit circle at $M_\infty = 0{\cdot}5$: —+—, present method, O-grid, 50×15; —○—, present method, O-grid, 60×20; —□—, full-potential finite-volume solution (Salas 1982).

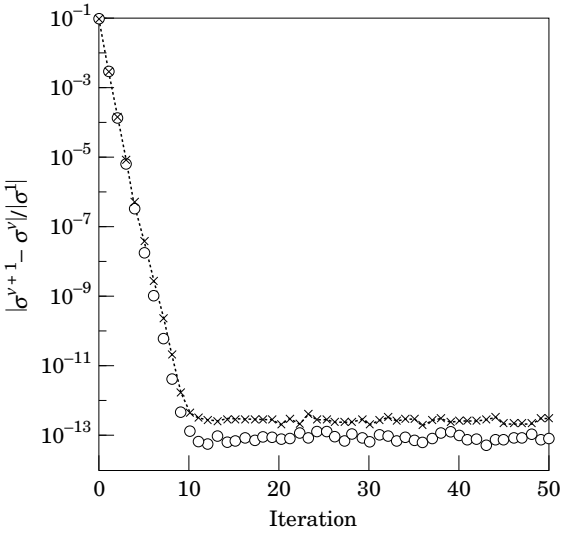

Figure 8. Time history of the iterative procedure for the convergence of σ. Test case of Figure 7: —○—, O-grid, 50×15; — + —; — − —, O-grid, 60×20.

$M_\infty = 0{\cdot}5$. The integral solution for two different mesh sizes is compared to finite volume full-potential solution due to Salas (1982). In this particular case, no Euler solutions are considered as reference results, since the strength of the shock yields a strong entropy jump; in this condition, the potential and Euler model are no longer comparable. The discontinuity in pressure predicted by the integral method appears as a jump, confined within one single element. The agreement with the finite–volume result is quite good in terms of shock position and intensity. Note that the convergence of the iteration to the steady-state solution is very fast and monotonic (Figure 8).

6.3. Effect of the Grid

Next, in order to study the effect of the grid type, we consider a non-lifting NACA 0012 airfoil at $M_\infty = 0{\cdot}82$. An H-type mesh, stretched and not uniformly distributed is used in the computation; the number of field elements is 50×20, and equations (14) and (18) are used for the artificial dissipation scheme. In order to clarify the issue of the sharpness of the shock, the velocity potential distributions obtained with two boundary integral approaches are presented in Figure 9; the shock appears as a sharp discontinuity for the potential slope. This sharpness is partially lost because of the smearing introduced by the numerical discretization used to evaluate the pressure from the potential. In Figure 10 the pressure distribution is compared to finite volume solution of both full-potential and Euler equations (in this case the comparison with the Euler solution is meaningful, because the shock is relatively weak and hence the entropy jump introduced by the shock is negligible). Note that the pressure-coefficient distribution obtained using equation (12) reveals, after the sonic point, some differences with respect to the reference results. This lack of accuracy, confined within the supersonic region of the domain, may be due to the different impact of the artificial dissipation schemes used in the two formulations [see, e.g., Iemma (1994)]. The convergence rate to the steady state (Figure 11) is lower than in the preceding case (in our experience the H-type grid, used for these results, appears to yield the lowest rate of convergence of the iteration scheme).

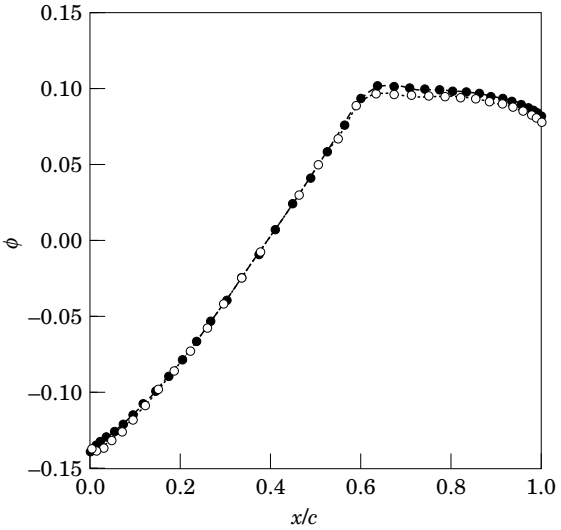

Figure 9. Velocity potential distribution on a NACA 0012 airfoil at $M_\infty = 0{\cdot}82$, and angle of attack $\alpha = 0°$: —○—, present method, equation (10); —●—, present method, equation (13).

In order to overcome this problem, a new grid geometry has been introduced for the calculation of the nonlinear field sources. The effects of the new geometry are shown in Figures 12 and 13. The first picture depicts the pressure distribution for the same test case of Figure 10. The introduction of the C-type grid allows for the use of a much higher number of surface elements, and allows for the convergence analysis of the method also in the supercritical range (with the H-type field grid, the convergence of the iterative procedure was very difficult with more than 45 panels along the chord). The solution of Figure 12 reveals a much more satisfactory behaviour in the vicinity of the shock, when compared to that obtained with the H-type grid (Figure 10). In

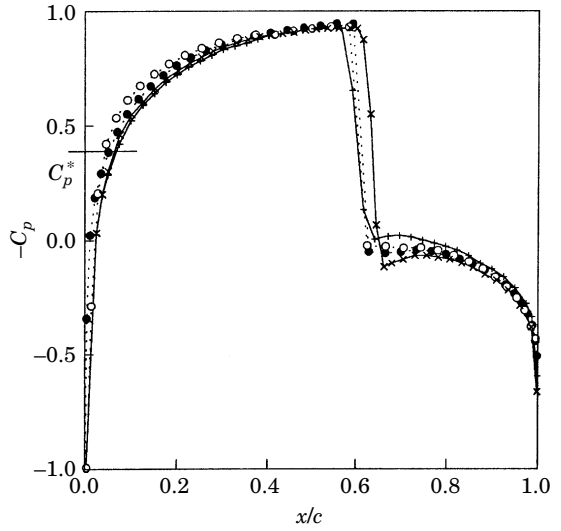

Figure 10. Pressure coefficient distribution on a NACA 0012 airfoil at $M_\infty = 0{\cdot}82$, and angle of attack $\alpha = 0°$: —●—, present method, equation (10), H-grid 35×10; —○—, present method, equation (13), H-grid 33×10; — × —, full-potential finite-volume solution [Salas, from Hirsh (1990)]; — + —, euler finite-volume solution [Salas, from Hirsh (1990)].

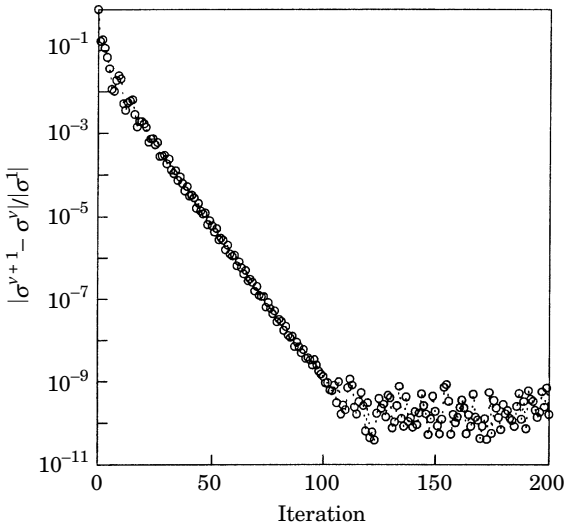

Figure 11. Time history of the iterative procedure. Test case of Figure 10.

addition, the rate of convergence is higher, and the convergence history of the nonlinear iterative process (Figure 13) is smoother. The nonlinear iterative process remains stable for much finer meshes, making possible the convergence analysis of the method also in the transonic range.

6.4. Convergence of Shock Location

The parameter used to assess convergence in the supercritical analysis is the position of the shock along the chord of a NACA 0012 airfoil at $M_\infty = 0{\cdot}82$. The reference result is obtained by a Jameson-type scheme using a finite-volume formulation for the full-potential model. The limit value for the shock position predicted by the BIEM

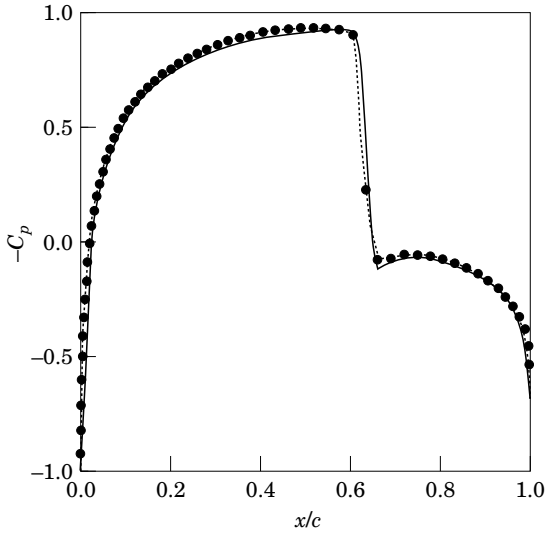

Figure 12. Pressure coefficient distribution on a NACA 0012 airfoil at $M_\infty = 0{\cdot}82$, and angle of attack $\alpha = 0°$: —●—, present method, equation (10), C-grid 70×20; — × —, full-potential finite-volume solution [Salas, from Hirsh 1990].

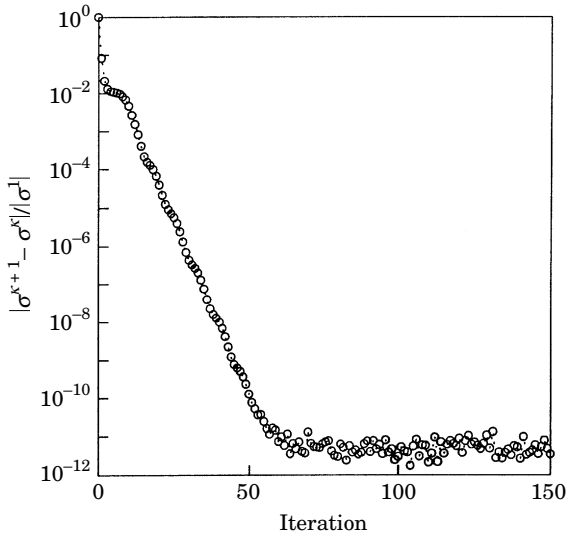

Figure 13. Time history of the iterative procedure. Test case of Figure 12.

formulation is obtained by means of extrapolation of the solution for the number of grid elements N tending to infinity. Specifically, the position of the shock for four different mesh sizes has been obtained by means of a rational function extrapolation of the potential in the vicinity of the shock, as shown in Figure 14. [The shock profile appears to be smooth as in a viscous shock [see, e.g., Serrin (1959)] maybe because of the artificial viscosity; thus the smoothed points are not utilized in the extrapolation procedure.] The values of the position of the shock obtained with the above procedure have been used as the basis of a Richardson extrapolation (see, e.g., Press *et al.* 1986)

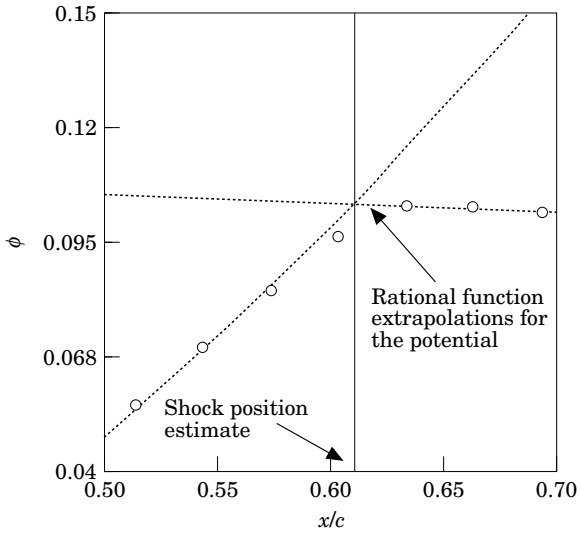

Figure 14. Shock position estimation from the velocity potential distribution: ○, value of ϕ computed at the control points; – – – –, rational function extrapolation of the potential across the shock.

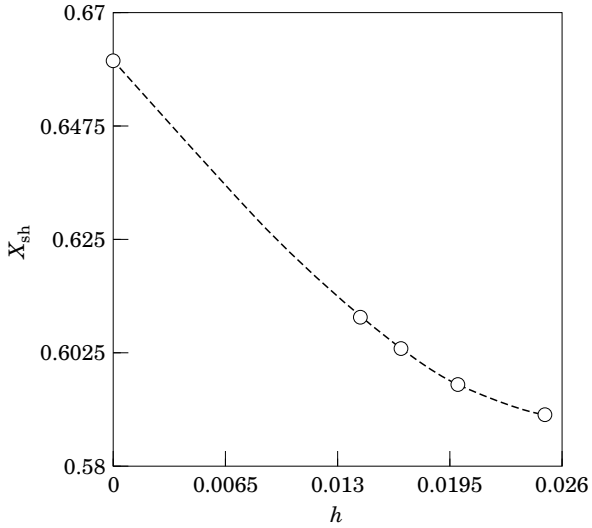

Figure 15. Extrapolation of the shock position for $N \to \infty$ ($h \to 0$).

in order to evaluate the limit solution for $h = 0$ (see Figure 15). In Figure 16, the result of the convergence analysis ($x_{sh} = 0{\cdot}6608$) has been compared with a fine grid volume solution obtained with the finite-volume code FLO36. Note that the reference solution has been obtained with a mesh size of 192×64, whereas the grids used for the extrapolation of the BEM solutions are, respectively, 40×5, 50×10, 60×20, and 70×30. The limit solution of the BEM method appears to be in excellent agreement with the finite volume solution.

6.5. Dissipation Schemes

Next, consider the effects of additional dissipation schemes. As mentioned above, in all the results presented the dissipative effects are introduced in the form of *nonlinear artificial viscosity* for the scheme in equation (11), and using the *flux-upwinding* technique, for that of equation (12). Two additional schemes have been applied to equation (11), in order to verify the applicability to a boundary integral formulation of concepts inspired by other CFD methods. In particular, dissipation is included as *artificial compressibility,* or in the form of *linear artificial viscosity.*

The results are presented in Figure 17. The test case deals with a biconvex parabolic airfoil, with thickness ratio 0·2, at $M_\infty = 0{\cdot}82$. Since the concept of modified density has been widely investigated in the past within the framework of the finite-element method, a finite-element solution for the full-potential equation is used as reference result (Kinney 1989). The pressure coefficient distribution presents a shock discontinuity, which appears sharper for the integral solution. The agreement is good for both formulations, even if the artificial compressibility approach presents a slight overestimation of the pressure distribution in the vicinity of the shock. Furthermore, the latter approach, which is nonlinear, presents a slower convergence of the iteration to the steady state, as shown in Figure 18. Note that in both cases we used $\mu(M)$ as in equation (15) with $\lambda = 100$ and $M_0 = 1$.

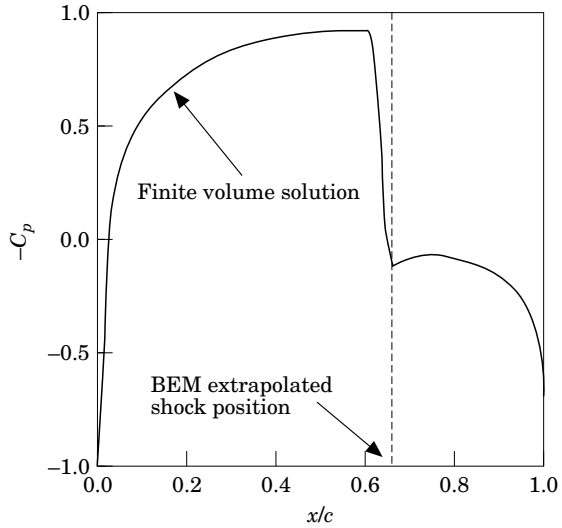

Figure 16. Comparison of the shock position extrapolated for $h \to 0$ with a fine grid, finite-volume solution.

6.6. Grid Independence

As already mentioned, the boundary integral formulation presents several features particularly appealing for design applications. In the present paper we would like to emphasize that the solution of the method appears to be almost independent of the geometry of the grid built around the body in order to evaluate the nonlinear field source of equation (9). This is true also in the transonic range, where other methodologies are usually very sensitive to small perturbations of the grid geometry.

Figures 19 and 20 present some preliminary results obtained for a NACA 0012 airfoil in transonic regime ($M_\infty = 0{\cdot}82$). The pressure distribution along the chord is evaluated

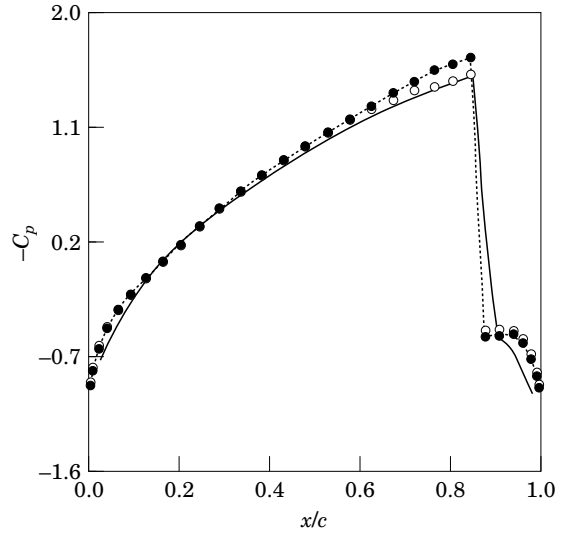

Figure 17. Influence of artificial dissipation schemes. Pressure coefficient distribution on a biconvex parabolic airfoil with 20% thickness, at $M_\infty = 0{\cdot}82$, and angle of attack $\alpha = 0°$: —○—, present method with artificial density; —●—, present method with artificial mass generation; ——, finite-element solution.

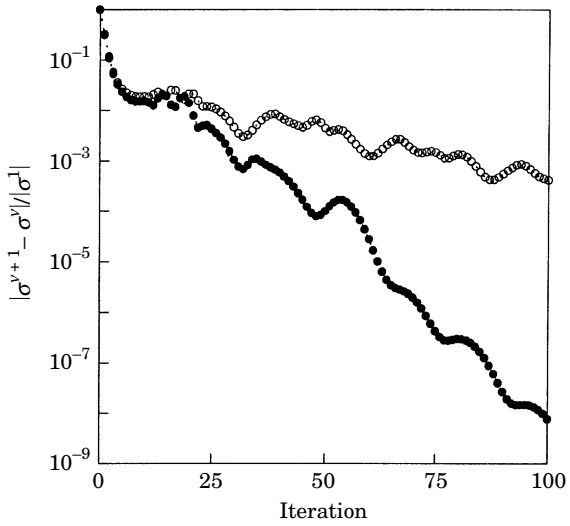

Figure 18. Time history of the iterative procedure for the convergence of σ. Test case of Figure 16: —○—, present method with artificial density; —●—, present method with artificial mass generation.

using four different field grids for the same configuration. In particular, the results obtained with a body-fit grid constructed around the NACA 0012 airfoil, are compared to those obtained using the grids constructed, respectively, around NACA 0009, NACA 0010, and NACA 0011 airfoils. Not only the solution (Figure 19), but also the convergence histories to the steady state (Figure 20) are virtually the same in the four cases. This result yields interesting considerations for the application of the present formulation to the design process. Indeed, the low sensitivity of the solution to the geometry of the field grid would allow the designer to modify the shape of the surface of the body without need for a re-evaluation of the geometry of the grid used for the aerodynamic numerical simulation.

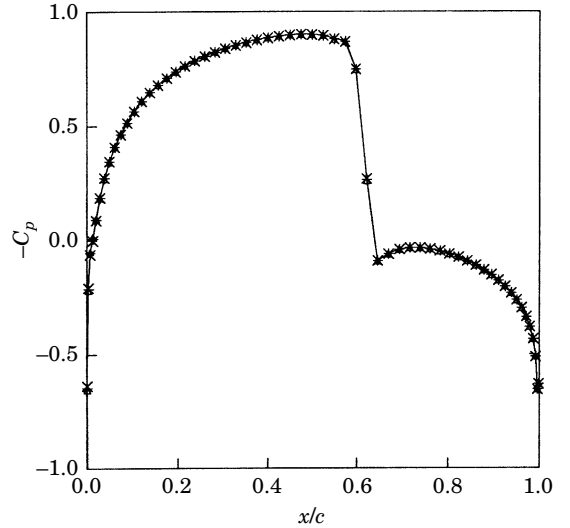

Figure 19. Grid independence. Pressure coefficient distribution on a NACA 0012 airfoil, at $M_\infty = 0{\cdot}82$, and angle of attack $\alpha = 0°$: ——, field grid built around the NACA 0012 geometry; —□—, field grid built around a NACA 0011; — + —, field grid built around a NACA 0010; — × —, field grid built around a NACA 0009.

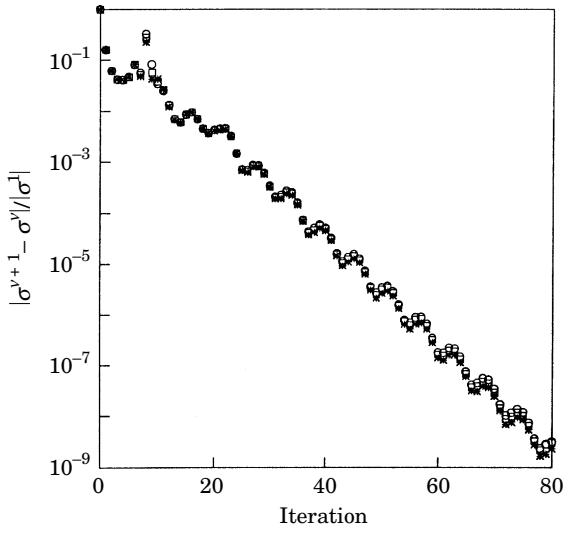

Figure 20. Time history of the iterative procedure. Test cases of Figure 18 (the meaning of symbols is the same as in that figure).

7. CONCLUDING REMARKS

A boundary integral equation method for the analysis of two-dimensional steady transonic potential flows has been presented. The formulation is obtained as the limiting case of the unsteady three-dimensional one, and the iterative method used to obtain steady-state results is a pseudo-time-accurate technique. The emphasis has been posed on the validation of the methodology with respect to other numerical methods for the full-potential and (when applicable) Euler equations. Comparisons with classical CFD methods reveal good agreement in both the subcritical and supercritical regimes. Shocks, when they occur, are sharp and correctly located. These are captured by means of the introduction of artificial dissipation in the supersonic region. Different schemes for the artificial viscosity as well as different grid types are analysed and assessed. The results of the convergence analysis are in very good agreement with accurate numerical results obtained with other numerical methods. In particular, for subsonic nonlinear flows the integral solution converges to the solution of the Euler equation, whereas in supercritical flows the shock position extrapolated from the solutions of the present method converges to that predicted by a fine-grid solution of the full-potential equation obtained with the finite-volume code FLO36.

The methodology presents several characteristics which are of particular interest from the point of view of aeronautical design. In particular, the formulation requires the discretization only of the portion of the fluid volume surrounding the body surface. Finally, the solution of the method is almost insensitive to modifications of the geometry of the field grid; this represents a highly desirable feature in those applications where repeated calculations are required, such as optimal design.

ACKNOWLEDGEMENTS

This work was partially supported through a contract from AGUSTA S.p.A. to the University of Rome III, and through a postdoctoral fellowship to Dr. U. Iemma.

References

DADONE, A. 1986 Computation of transonic steady flows using a modified lambda formulation. In *Numerical Simulation of Compressible Euler Flows* (eds A. Dervieux, B. Van Leer, J. Periaux & A. Rizzi), GAMM Workshop, pp. 122–137. Braunschweig: Vieweg & Sohn.

EBERLE, A. 1977 A finite element method for the solution of transonic potential flows around airfoils. NASA Technical Memorandum 75324.

ENGQUIST, B. & OSHER, S. 1980 Stable and entropy satisfying approximation for transonic potential flow calculation. *Mathematics of Computation* **34** number 149, 45–75.

GENNARETTI, M., IEMMA, U. & MORINO, L. 1995a A boundary integral method for unified transonic aerodynamics and aeroacoustics of hovering rotors. In *AGARD Conference on Aerodynamics and Aeroacoustics of Rotorcraft,* number 552, Berlin, Germany.

GENNARETTI, M., IEMMA, U. & MORINO, L. 1995b Recent developments on a BEM for aerodynamics and aeroacoustics of rotors. In *21st European Rotorcraft Forum Proceedings,* Saint Petersburg, Russia.

HAFEZ, M. M., SOUTH, M. M. & MURMANN, E. M. 1978 Artificial compressibility method for the numerical solution of the full potential equation. *AIAA Journal* **17,** 838–844.

HIRSCH, C. 1990 *Numerical Computation of Internal and External Flows. Computational Methods for Inviscid and Viscous Flows,* Volume 2. New York: John Wiley & Sons.

HOLST, T. L. & BALLHAUS, W. F. 1979 Fast, conservative schemes for the full potential equation applied to transonic flows. *AIAA Journal* **17,** 145–152.

IEMMA, U. 1994 Metodi integrali in aerodinamica transonica. Doctoral thesis in aerospace engineering (in italian), Università degli Studi di Roma *La Sapienza,* Roma.

IEMMA, U., GENNARETTI, M. & MORINO, L. 1993 Boundary element method for unified transonic aerodynamic and aeroacoustic analyses of rotors. In *19th European Rotorcraft Forum Proceedings,* Cernobbio, Italy.

IEMMA, U., MASTRODDI, F., MORINO, L. & PECORA, M. 1991 A boundary integral formulation for unsteady transonic potential flow. In *AGARD Specialists' Meeting on Transonic Unsteady Aerodynamics and Aeroelasticity,* number 507, San Diego, California.

IEMMA, U. & MORINO, L. 1994 Transonic analysis using a boundary element method. In *10th ICAS Conference Proceedings,* pp. 2793–2803, Anaheim, California, U.S.A.

JAMESON, A. 1974 Iterative solutions of transonic flows over airfoils and wings, including flows at Mach 1. *Communications in Pure and Applied Mathematics,* number 27, pp. 283–309.

JAMESON, A. 1975 Transonic potential flow calculation using conservation form. In *AIAA Second Computational Fluid Dynamics Proceedings,* pp. 148–161, Hartford Connecticut, U.S.A.

KANDIL, O. A. & HU, H. 1988 Full-potential integral solution for transonic flows with and without embedded Euler domains. *AIAA Journal* **26,** 1079–1086.

KINNEY, D. J. 1989 Finite Element Simulation of Compressible Inviscid and Viscous Flows. Ph.D. thesis, University of California, Davis, CA.

LERAT, A. & SIDES, J. 1986 Implicit transonic calculations without artificial viscosity or upwinding. In *Numerical Simulation of Compressible Euler Flows* (eds A. Dervieux, B. Van Leer, J. Periaux & A. Rizzi), GAMM Workshop, pp. 227–250, Braunschweig, Vieweg & Sohn.

MORINO, L. 1974 A general theory for unsteady compressible potential aerodynamics. NASA Contractor Report CR-2464.

MORINO, L. 1993 Boundary integral quations in aerodynamics. *Applied Mechanics Reviews* **46,** 445–466.

MORINO, L., GENNARETTI, M., IEMMA, U. & MASTRODDI, F. 1992 Boundary integral transonics for wings and rotors. *Aerotecnica Missili e Spazio* **71,** number 1/2, pp. 52–61.

MORINO, L. & IEMMA, U. 1993 Boundary integral equations and conservative dissipation schemes for full-potential transonic flow. *Computational Mechanics* **13,** 90–100.

MORINO, L., IEMMA, U. & MASTRODDI, F. 1994 BEM, transonics and aeroelasticity. In *ECCOMAS Conference Proceedings,* pp. 1123–1132, Stuttgart, Germany.

MURMAN, E. M. 1974 Analysis of embedded shock waves calculated by relaxation methods. *AIAA Journal* **12,** 626–633.

MURMAN, E. M. & COLE, J. D. 1971 Calculation of plane steady transonic flows. *AIAA Journal* **9,** 114–121.

NIXON, D. 1974 Transonic flow around symmetric aerofoils at zero incidence. *Journal of Aircraft* **11,** 122–124.

NIXON, D. 1978 Calculation of unsteady transonic flows using the integral equation method. *AIAA Journal* **16,** 976–983.

OSHER, S. 1982 Shock modelling in aeronautics. In *Numerical Methods for Fluid Dynamics* (eds K. W. Morton and M. J. Baines), pp. 1179–218. London: Academic Press.

OSWATITSCH, K. 1950 Die Geschwindigkeitsverteilung ab symmetrische Profilen beim auftreten lokaler Überschallgebiete. *Acta Physica Austriaca* **4,** 228–271.

PIERS, W. J. & SLOOF, J. W. 1979 Calculation of transonic flow by means of shock-capturing field panel method. AIAA Paper 79-1459.

PRESS, W. H., FLANNERY, B. P., TEUKOLSKY, S. A. & VETTERLING, W. T. 1986 *Numerical Recipes. The Art of Scientific Computing.* New York: Cambridge University Press.

ROETTERGERMANN, A. & WAGNER, S. 1995 Compressible potential flow around a helicopter rotor. In *Computational Mechanics '95, Proceedings of the International Conference on Computational Engineering Science* (eds S. N. Atluri, G. Yagawa, & T. A. Cruse), Vol. 2, pp. 2915–2920), Hawaii, U.S.A.

ROETTGERMANN, A. & WAGNER, S. 1995 Cost efficient calculation of compressible potential flow around a helicopter rotor including free fortex sheet by a field panel method. In *AGARD Conference on Aerodynamics and Aeroacoustics of Rotorcraft,* number 552, Berlin, Germany.

SALAS, M. D. 1982 Recent developments in transonic Euler flow over a circular cylinder. NASA Technical Memorandum 83282, Langley Research Center, Hampton, Virginia, U.S.A.

SERRIN, J. 1959 Mathematical principle of classical fluid mechanics. In *Fluid Dynamics I* (eds S. Flügge & C. Truesdell), *Encyclopedia of Physics,* Vol. VIII/1, pp. 125–263. Berlin: Springer-Verlag.

SINCLAIR, P. M. 1986 An exact integral (field panel) method for the calculation of 2-dimensional transonic potential flow around complex configuration. *Aeronautical Journal* **90,** 227–236.

SINCLAIR, P. M. 1988 A three-dimensional field integral method for the calculation of transonic flow on complex configuration—theory and preliminary results. *Aeronautical Journal* **92,** 235–241.

SPREITER, J. R. & ALBERTA ALKSNE, A. 1954 Theoretical prediction of pressure distribution on nonlifting airfoils at high subsonic speed. NACA Technical Note 3096.

TSENG, K. 1983 *Nonlinear Green's Function Method for Transonic Potential Flows.* Ph.D. thesis, Boston University, Boston, Mass., U.S.A.

TSENG, T. 1984 Applications of the Green's function method for two- and three-dimensional steady transonic flows. AIAA Paper 84-0425.

TSENG, K. & MORINO, L. 1982 Nonlinear Green's function method for unsteady transonic flows. In *Transonic Aerodynamics* (ed. D. Nixon), number 81 in *Progress in Astronautics and Aeronautics,* pp. 565–603.

ZHANG, H. L., ROETGGERMANN, A. & WAGNER, S. 1995 Field panel method with grid stretching technique for solving transonic potential flow around arbitrary airfoils. *Computational Mechanics* **15,** 384–393.